Analyzing powers for πp elastic scattering between 57 and 139 MeV

J. D. Patterson,[1,*] G. J. Hofman,[1,†] J. T. Brack,[1] P. Camerini,[5] J. Clark,[8] P. P. J. Delheij,[2] L. Felawka,[2] E. Fragiacomo,[5] E. F. Gibson,[7] N. Grion,[4,5] B. Jamieson,[3] E. L. Mathie,[6] R. Meier,[9] D. Ottewell,[2] R. J. Peterson,[1] K. Raywood,[2] R. A. Ristinen,[1] R. Rui,[4,5] M. E. Sevior,[8] G. R. Smith,[2,‡] R. Tacik,[6] G. Tagliente,[3] G. J. Wagner,[9] and D. M. Yeomans[6]

[1]*University of Colorado, Boulder, Colorado 80309-0446*

[2]*TRIUMF, Vancouver, British Columbia, Canada V6T 2A3*

[3]*Department of Physics and Astronomy, University of British Columbia, Vancouver, British Columbia, Canada V6T 2A6*

[4]*Istituto Nazionale di Fisica Nucleare, I-34127 Trieste, Italy*

[5]*Dipartimento di Fisica dell'Universita' di Trieste, I-34127 Trieste, Italy*

[6]*University of Regina, Regina, Saskatchewan, Canada S4S 0A2*

[7]*California State University, Sacramento, California 95819*

[8]*School of Physics, University of Melbourne, Parkville, Victoria 3052, Australia*

[9]*Physikalisches Institut, Universität Tübingen, Tübingen 72076, Germany*

(Received 26 May 2002; published 29 August 2002)

Analyzing powers for πp elastic scattering at bombarding energies below the $\Delta(1232)$ resonance were measured at TRIUMF using the CHAOS spectrometer and a polarized spin target. This work presents π^- data at six incident energies of 57, 67, 87, 98, 117, and 139 MeV, and a single π^+ data set at 139 MeV. The higher energy measurements cover an angular range of $72° \leqslant \theta_{\text{c.m.}} \leqslant 180°$ while the lower energies were limited to $101° \leqslant \theta_{\text{c.m.}} \leqslant 180°$. There is a high degree of consistency between this work and the predictions of the VPI/GWU group's SM95 partial wave analysis.

DOI: 10.1103/PhysRevC.66.025207 PACS number(s): 13.75.Gx, 24.70.+s, 25.80.Dj

I. INTRODUCTION

The value of the pion-nucleon sigma term ($\Sigma_{\pi N}$), an explicit measure of chiral symmetry breaking due to nonzero quark masses, has been in dispute in part due to lack of high quality, consistent measurements of low-energy pion-nucleon observables. Chiral perturbation theory has related $\Sigma_{\pi N}$ to the baryon mass spectrum and hence to the strange (sea) quark content $y = 2\langle p|\bar{s}s|p\rangle / (\langle p|\bar{u}u + \bar{d}d|p\rangle)$ of the nucleon wave function. The πN observables can be related to the $\Sigma_{\pi N}$ term using extrapolations of the scattering amplitudes to the subthreshold ($\nu = 0$, $t = 2\mu^2$) Cheng-Dashen point [1]. Estimates of the $\Sigma_{\pi N}$ term from the Karlsruhe (KH80) partial wave analysis (PWA) by Hohler [2] and Koch and Pietarinen [3], which use exclusively pre-meson-factory data, imply $\Sigma_{\pi N} = 64 \pm 8$ MeV ($y = 0.2 \pm 0.2$). Newer analysis using the VPI/GWU PWA [4], which incorporates modern pion-nucleon measurements, have raised this value to $\Sigma_{\pi N} = 84 \pm 5$ MeV ($y = 0.5 \pm 0.1$) [5]. To properly constrain future phase shift analyses and to reduce the uncertainties in the extrapolations, accurate low-energy measurements of both differential cross sections and spin observables are needed. In particular, both π^- analyzing powers near 50 MeV and forward scattering $\pi^\pm$ differential cross sections near 30 MeV are critical for the extrapolations.

Additional interest arises from possible isospin breaking in the pion-nucleon *S*-wave amplitude, which has been inferred in the analysis of low-energy πN data by Gibbs *et al.* [6] and, more recently, by Matsinos [7]. Both analyses, which rely exclusively on data below 100 MeV, report an approximate 7% effect in the difference between elastic and single charge exchange real part *S*-wave amplitudes.

A large set of back-angle, pion-nucleon differential cross section data below 100 MeV exists. Measurements in the forward regions at very low energies is experimentally challenging and little data are available at present. Such measurements are the subject of CHAOS experiment *E*778 [8], presently under analysis.

It is advantageous to measure spin observables, such as analyzing powers (A_y), rather than additional differential cross sections. Analyzing powers are the results of an interference between the spin-flip (G) and spin-nonflip (H) amplitudes and hence sensitive to smaller, nonresonant partial waves. Moreover, the analyzing power

$$A_y = \frac{\sigma^\uparrow - \sigma^\downarrow}{P^\downarrow \sigma^\uparrow + P^\uparrow \sigma^\downarrow} = \frac{Y^\uparrow / N^\uparrow - Y^\downarrow / N^\downarrow}{P^\downarrow Y^\uparrow / N^\uparrow + P^\uparrow Y^\downarrow / N^\downarrow} = \frac{2\,\text{Im}(GH^*)}{(|G|^2 + |H|^2)} \tag{1}$$

is subject to quite different systematic errors. Usual cross section normalization quantities such as solid angle, number of target nuclei, pion decay fraction, and detection efficiency cancel out, leaving only the πp yield ($Y^{\uparrow\downarrow}$), the beam normalization ($N^{\uparrow\downarrow}$), target polarization ($P^{\uparrow\downarrow}$), and background as the sensitive quantities. The $\uparrow\downarrow$ arrows indicate the z com-

*Present address: Jet Propulsion Laboratory, California Institute of Technology, Pasadena, CA. Email address: Jeffrey.D.Patterson@jpl.nasa.gov

†Present address: TRIUMF, Vancouver, BC, Canada V6T 2A3. Email address: gertjan@triumf.ca

‡Present address: Jefferson Lab, Newport News, VA 23006.

ponent of the spin of the target protons, which is perpendicular to the pion scattering plane.

Previous analyzing power measurements were focused on energies around the $\Delta(1232)$ resonance. The TRIUMF data of Sevior *et al.* [9] cover a large energy range (98–263 MeV), but a limited angular range. There are seven additional data sets, published by Alder *et al.* [10] (π^-), Raue *et al.* [11] (π^+), and Amsler *et al.* [12] (π^+) above 95 MeV. More recently, Wieser *et al.* [13] published four data points at 68.3-MeV π^+. Finally, in a measurement using the same experimental setup reported here, data were taken for a number of energies across the $\Delta(1232)$ resonance [14]. These data were normalized at one energy, 139-MeV π^+, to the statistically precise data of Sevior *et al.* Improvements of the polarized target now allowed extension of these measurements below 100 MeV, as well as an independent verification of the polarization normalization.

With the target polarization problems resolved, new, low-energy analyzing power data in the π^- channel were collected with the CHAOS spectrometer and are presented here.

II. EXPERIMENTAL APPARATUS

A. CHAOS

All data were collected using the CHAOS spectrometer and a dedicated spin-polarized target [15] in the $M11$ pion channel at TRIUMF. A detailed description of CHAOS can be found in Ref. [16] and references therein, but the components crucial to this work are described below.

The spectrometer consisted of four low-mass, cylindrical concentric tracking chambers and layers of particle identification counters immersed in a vertical magnetic field provided by a cylindrical dipole magnet with an open geometry. The inner two wire chambers (WC1 and WC2) are proportional vertex chambers with radii of 11.5 and 22.3 cm, respectively. A drift chamber (WC3 [17]) was positioned at a radius of 34.4 cm. The struck-wire information from WC1, WC2, and WC3 was used in a second-level trigger [18]. The drift time information from WC3 was digitized and used to improve off-line tracking, but was not part of the trigger system. Positioned in the tail of the magnetic field at a radius of 62–66 cm was a vector drift chamber (WC4). This chamber, with 100 cells of eight anode wires each, vastly improved the particle tracking and momentum resolution. Surrounding the WC4 detector were two layers of plastic scintillation counters and an outer layer of lead-glass Cherenkov counters. The counters were arranged in 20 blocks, each 18° wide. The ΔE_1 counters were 3-mm-thick NE110 plastic and faced the target at a radius of 71 cm. Behind each ΔE_1 counter were two adjacent 9°-wide scintillators ΔE_{2l} and ΔE_{2r} made of 12-mm-thick NE110 plastic. Data from ΔE_2 and Cherenkov detectors were not used in the analysis of this experiment. The ΔE_1 counter modules subtended $\pm 7°$ in the vertical direction and defined the out-of-plane acceptance. In the horizontal scattering plane the acceptance was nominally 360°, except for a single 18° section removed at the beam entrance.

A four-element scintillation counter hodoscope ($S1$) defined the incident beam, and also provided the time reference for all the readout electronics. The low rate WC3 was switched off in the incoming and outgoing beam regions. A 54° angular section of WC4 was replaced with a 36° section, leaving an 18° gap in the incoming beam region. Three cells were deactivated in the outgoing beam region. $S1$ was situated where WC4 would have been in the incoming beam region, at a radius of approximately 65 cm. All the incident beam pions were detected by the proportional chambers WC1 and WC2. Knowledge of the average beam momentum and the magnetic field in conjunction with the WC1 and WC2 hit information allowed track reconstruction of the incident pions to the target at the center of the magnet.

Pions scattered from the target were typically detected by all four wire chambers, as shown in Fig. 1. At higher incident beam energies, the recoil proton is also tracked through all detectors. At the two lowest pion energies, the detection of these low momentum protons was limited to two or three inner chambers. The protons that were only detected by the inner chambers are termed short-track protons.

The magnitudes of the magnetic fields were chosen to provide the greatest curvature for the scattered pions without trapping the lowest-momentum scattered particles. The field was scaled with the incident momentum in order to maintain a similar scattering geometry at all incident beam energies. For this experiment, a value of $p/B \approx 153$ MeV/cT was used.

The $M11$ beam channel was tuned to pion energies of 138.9, 116.8, 98.0, 87.2, 66.9, and 57.2 MeV at the center of the polarized target. The energy determination was based on time-of-flight measurements performed for a previous experiment [19] in this channel. The systematic error in the mean pion kinetic energy was estimated to be 0.3%. However, the low π^- particle flux from the channel necessitated a relatively large momentum bite, varying from 1% to 4%. The corresponding beam energy widths are quoted with the tabulated results. The consequence of the energy distribution is discussed in Sec. IV B.

B. Trigger requirements

Event filtering was accomplished in CHAOS by three levels of on-line triggering. The first-level trigger (1LT) [20] was based on the multiplicity of hits in the ΔE_1 counters. The second-level trigger (2LT) [18] analyzed the data from WC1, WC2, and WC3 and made decisions based on the possible number of scattered tracks, their polarity, momentum, and the distance of closest approach to the center of CHAOS. The third level (3LT) was a software trigger running on a VMEbus data acquisition computer. Data were written to permanent storage using the MIDAS [21] acquisition software.

Each of the ΔE_1 counters was potentially an active contributor to the hit multiplicity that formed the output of the 1LT. For the higher-energy measurements where the recoil proton was energetic enough to reach the counter blocks for a large range of scattering angles, the minimum event multiplicity was set to two hits (a ''doubles'' 1LT) but for the 67- and 57-MeV measurements, the hit multiplicity was reduced to only a single hit (''singles'' 1LT). In both cases, hits in the ΔE_2 counters were not demanded since many of the low-energy particles were stopped in the ΔE_1 counters. Note that

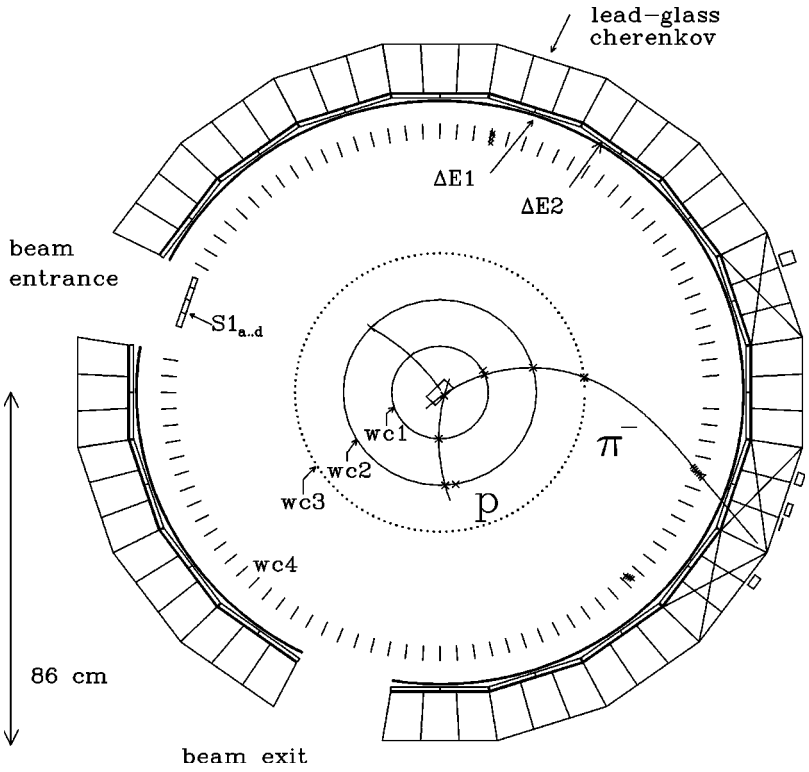

FIG. 1. Typical $\pi^- p$ coincidence event at 57 MeV. The beam pion enters through the four-segment scintillator $S1$, is detected in wire chambers WC1 and WC2, and traced to the target at center. The scattered pion traverses all four chambers and stops in the scintillators ΔE_2 or in the lead-glass detectors. The recoil proton is detected in chambers WC1 and WC2 only, corresponding to a short-track event.

the 1LT logic could not distinguish the geometric location of the hits, a task which was left to the third-level software trigger. As for all CHAOS experiments, one of the 18° blocks was removed to allow the unhindered entry of the beam into the spectrometer and, similarly, one block was removed at the beam exit. A consequence of removing the counter block at the beam exit is to create a hole in the spectrometer acceptance, exactly where most forward recoil protons would be detected. A special counter block consisting of only the ΔE_1 and ΔE_2 counters was therefore inserted at the beam exit. Pulse height discrimination was used to allow protons to participate in the trigger of an event, while pions could not.

A passed 1LT started the second-level trigger, and provided the gate for the digitization systems and the stop for the drift chamber timing signals. The 2LT performed a triple computational loop over all struck-wire numbers from the three inner wire chambers (WC1–WC3). For this experiment, the 2LT was operated in one of two modes, labeled standard or short track, depending upon the incident momentum. Standard mode was typically used when the 1LT was set to ''doubles.'' In standard mode, the trigger searches for candidate tracks and performs cuts on the polarity and closest distance of approach to the target. The short-track mode was used when the 1LT was set to ''singles.'' In this mode, a single, positive polarity track (the recoil proton) was searched for in forward regions of WC1 and WC2, using the angle difference between the WC1 and WC2 hits. Further 2LT criteria for both the standard and short-track mode included valid hits in the incoming beam regions of WC1 and WC2. This condition efficiently eliminated events with muons from in-flight pion decay that entered CHAOS at the wrong angle with respect to the nominal beam axis.

The final, third-level (3LT) stage consisted of software requirements in the VME data acquisition computer, and performed event rejection based on the partial readout of the data. It is required that the time of flight of particles from the pion production target to $S1$ corresponds to pions, reducing electron and muon contamination. When in coincident trigger mode, it is also required for the 3LT that the hit combination in the ΔE_1 counters correspond to that expected from elastic πp scattering kinematics.

C. Spin-polarized target

A spin-polarized target [15] operating in frozen-spin mode was designed for use in the CHAOS spectrometer. The target was identical to that described in Ref. [14] except for the use of frozen butanol beads rather than a frozen slab. The target cell consisted of a $(30\times25\times5)$ mm^3 $(W\times H\times T)$ copper vessel of 25.4-μm wall thickness. The target material was a mixture of butanol (C_4H_9OH) and EHBA (Sodium Bis [2-ethyl-2-hydroxbuty-rato(2-)] oxochromate (V) monohydrate Cr (V)). The relative concentrations were 5×10^{19} molecules of EHBA to 1 cc of butanol. Water was added to the mixture in a 1:20 ratio by volume. Butanol beads approximately 1 mm in diameter were formed by freezing in liquid nitrogen. To obtain sufficiently long polarization relaxation times (>400 h), once polarized, the target temperature was kept below 100 mK. This was achieved using a standard dilution refrigerator technique. The mixing chamber surrounded the cell, with the ^{4}He/^{3}He interface immediately above the target cell. The refrigerator cooled the cell from 1.2 K to the operating temperature of 60–70 mK.

1. Polarization procedure

The CHAOS magnetic field served as the polarization holding field during the data acquisition, but it did not have

the required strength or the 1 in 10^4 homogeneity to serve as a polarizing magnet. A separate superconducting solenoid (PS), outside of CHAOS, provided the necessary homogeneous 2.5 T field for polarization. A third magnet, the holding coil (HC), also superconducting, was situated immediately above the butanol target cell inside the cryostat and was required only during transit of the cryostat from the polarizing magnet to the center of CHAOS.

The polarization procedure consisted of the following steps. The target was dynamically polarized in the PS, and the final polarization achieved was measured as described below. The PS was ramped from 2.5 T to ~0.3 T. The HC was then energized to provide ~0.3 T in its fringe field, and the target was raised about 50 cm until it cleared the top of the PS. The PS was then rolled clear and the target was lowered 1.4 m through the open 16-cm-diameter bore hole of the CHAOS magnet until it reached beam height. The CHAOS field was then ramped up to 0.3 T at the center, after which the HC was ramped off. The CHAOS field was finally ramped up to the field required for the πp scattering measurements. After completing the data taking, the same sequence was reversed.

The average loss of the polarization during this transportation sequence was determined from target nuclear magnetic resonance (NMR) measurements before and after data acquisition. Repeated trial round trips, in which the target was inserted and immediately extracted from the CHAOS magnet, showed that typical transit losses were 3–5 % of the original polarization. Polarization decay times at the operating field of CHAOS were always in excess of 400 h, resulting in negligible decay during the data recording.

2. NMR measurements

The magnitude of the target polarization was determined from measurements of the proton NMR signal. The NMR coil was a single wire loop, made of (1-mm-diameter) copper, coated with teflon and permanently embedded inside the target cell. It was part of an external two-arm *Q*-meter circuit, driven at the proton Larmor frequency (107.0 MHz at $B=2.508$ T). To increase the signal-to-noise ratio, the signal from the compensating arm was subtracted from that of the NMR arm containing the embedded coil. The combined signal was amplified, fed into a phase sensitive detector, and digitized. Since spin-spin interactions broaden the Zeeman absorption lines, the resonance frequency was scanned (in 512 steps of 2 kHz) around the Larmor frequency. The integrated NMR signal is proportional to the target polarization.

The standard technique to obtain an absolute calibration of the target polarization is to compare the integrated dynamic NMR signal area with the NMR signal obtained at some equilibrium temperature, where the polarization at the field H and temperature T is determined by the Boltzmann distribution. These thermal equilibrium (TE) signals were taken every 3 days. The magnetic field strength was determined from the NMR center frequency and the temperature ($\approx$1.2 K) from the ^{3}He vapor pressure was measured directly above the target cell.

To obtain background signals for the NMR measurement, the magnetic field was lowered by 3% to shift the Larmor frequency away from the resonance. Background signals were acquired over the same frequency range over which the real NMR signals were measured. The magnetic field was readjusted to 2.508 T and the foreground signal was measured over a frequency range wide enough to include off-resonance regions. Multiple foreground and background signals (usually 3–6) were averaged and the signal areas were then determined using the expression

$$A_{\text{therm}}=\sum_{i=1}^{512} S_i-(\alpha+\beta f_i)B_i+\gamma, \tag{2}$$

where S_i is the foreground signal at frequency f_i, B_i is the background signal, and α, β, γ are fitting parameters determined by minimizing the appropriate χ^2 over regions away from the resonance peak.

Typical polarizations achieved with this target are approximately 0.8. The NMR technique introduces an overall uncertainty of 3.7% in all the polarization measurements of this work. This systematic error is dominated by the variations in the background signal observed during the TE measurements.

III. DATA ANALYSIS

A. Beam normalization

To reduce systematic error, the target polarization was flipped while maintaining the beam energy. The time between spin flips of the target atoms depended upon which energy was currently being measured, but a typical run lasted three days. The 360° acceptance of CHAOS can be used to avoid the need for beam counting, a technique used and described earlier in Ref. [14]. The rotational symmetry inherent to the scattering of a spin-0 projectile from a spin-1/2 particle polarized perpendicular to the scattering plane requires

$$A_y(\theta)=-A_y(-\theta). \tag{3}$$

Since the CHAOS spectrometer measures most angles in the left ($0°<\theta_\pi<180°$) hemisphere simultaneously with those in the right hemisphere ($180°<\theta_\pi<360°$), Eq. (3) can be used to obtain the relative normalization of the spin-up and spin-down scattering yield. Let α be the ratio of all spin up to spin down normalization factors, including the beam counts $N^\uparrow$ and $N_\downarrow$ and pion decay and counting efficiencies. The analyzing power can then be written as

$$A_y=\frac{Y^\uparrow-\alpha Y^\downarrow}{P^\downarrow Y^\uparrow+\alpha P^\uparrow Y^\downarrow}, \tag{4}$$

where α can be fit by minimizing

$$\chi^2=\sum_i^{n/2}\frac{[A_y(\theta_i)+A_y(-\theta_i)]^2}{\delta A_y(\theta_i)^2+\delta A_y(-\theta_i)^2}, \quad 0°<\theta_i<180° \tag{5}$$

or

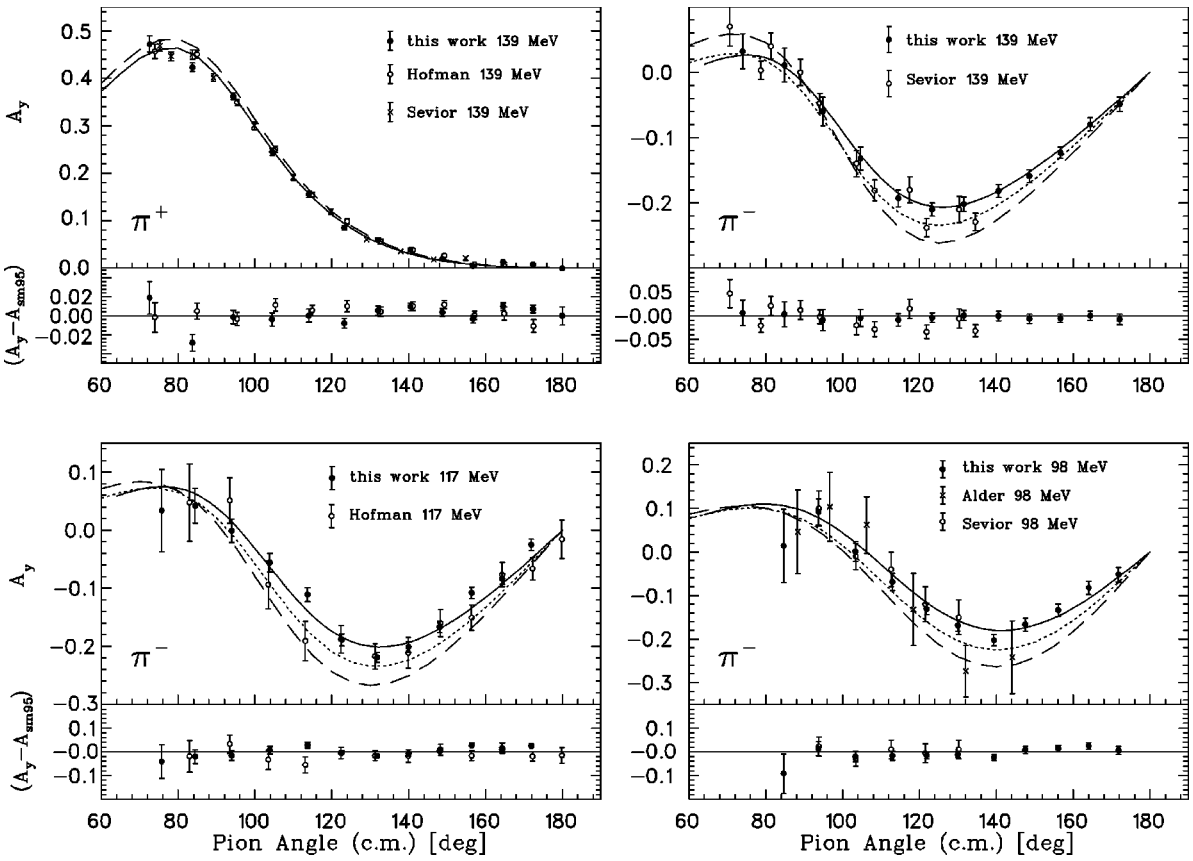

FIG. 2. The new analyzing powers compared to existing data sets for 139-, 117-, and 98-MeV π^- (Sevior *et al.* [9], Hofman *et al.* [14], and Alder *et al.* [10]) and 139-MeV π^+ (Sevior *et al.* [9] and Hofman *et al.* [14]). In each case the solid line is the SM95 phase-shift solution, the dotted line the SM02 solution, and the dashed line the KH80 solution. The lower graphs show, on a smaller scale, the SM95 solution subtracted from the new experimental analyzing powers.

$$\chi^2 = \sum_i^n \frac{[A_y(\theta_i) - A_p(\theta_i)]^2}{\delta A_y(\theta_i)^2}, \quad 0° < \theta_i < 360°, \qquad (6)$$

where n is the total number of data points (angles). The second expression, which uses some antisymmetric function A_p, such as an existing phase shift solution, is more convenient because it does not require all data at measured angles θ to have counterparts at $-\theta$ (due to missing trigger blocks or deadened chamber sections). The sensitivity of the results to the specific choice of antisymmetric functions was investigated and none was found. Furthermore, the tabulated values for analyzing powers use the (statistical) average of the values obtained at θ and $-\theta$, which is only weakly dependent on α.

The values of α ranged from 0.63 to 1.82, depending upon how much beam time was allotted to the spin-up and spin-down measurements, and contributed a systematic error to the measurements of approximately 0.5%. There is no further systematic error in the analyzing power attributed to the beam counting.

B. Particle identification

For the π^- data, particle identification was accomplished using the polarity of the found tracks. If multiple tracks for either or both polarities exist (which can occur when more than one pion exits the channel during the same primary beam burst), then the momentum and scattering angle of each track is calculated. Elastic kinematics are used to determine which negative polarity track to associate with the pion, and which positive one to identify with the proton, considering all combinations of tracks. For the single π^+ data set, the same methodology is employed, except that only positive pairs of tracks are considered for the final states.

C. Background reduction

Background reactions are expected from the carbon and oxygen in the butanol target, the ^{4}He/^{3}He coolant mixture, the target cell, and cryostat windows. For all the data presented here, the off-line analysis required identification of both a pion and recoil proton. This condition reduced the angular coverage but eliminated elastic scattering from $Z > 1$ nuclei and all other reactions that do not produce a pion and a proton in the final state. Kinematic cuts on the proton momentum and scattering angle and on the pion momentum as well as on the reaction vertex were used to isolate the elastic πp events. Only an insignificant number of three-body quasielastic events whose kinematics overlap the elastic πp kinematics and fell within the limited ($\pm 7°$) out-of-

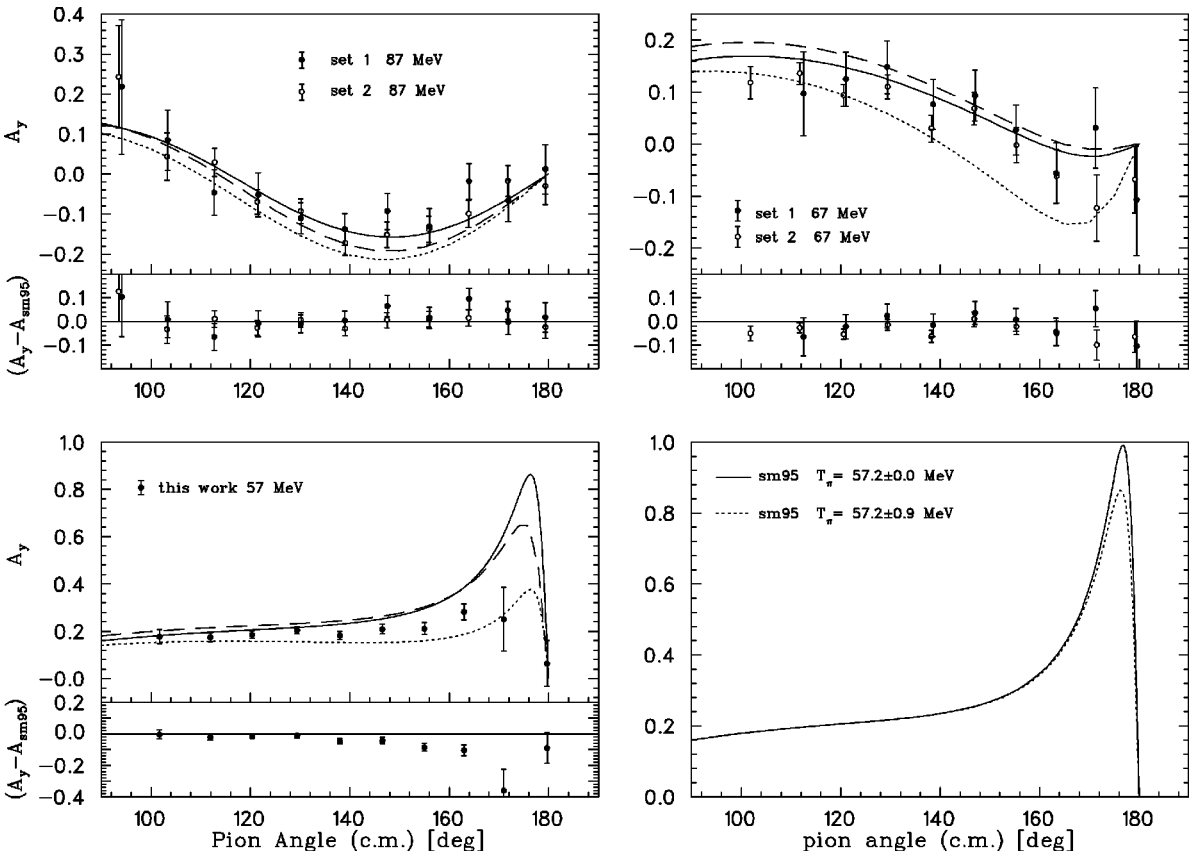

FIG. 3. The analyzing powers compared to phase shift solutions 87-, 67-, and 57-MeV π^-. In each case the solid line is the SM95 phase shift solution, the dotted line the SM02 solution, and the dashed line the KH80 solution. The lower graphs show the new experimental analyzing powers subtracted from the SM95 solution. The lower right panel illustrates the effect of convoluting the SM95 analyzing power predictions with the experimental beam energy distribution at 57.0±0.2 MeV $\pi^- p$. The effect is only significant at this incident pion energy.

plane acceptance were expected. To measure the quasielastic contribution to the spectrometer's signal, data from a carbon slab were obtained, and virtually no quasielastic events were found in the final analysis.

D. Scattering angle corrections

Due to the rapidly changing cross section and analyzing power across an angular bin, the value of A_y measured in an angular bin of width $\theta_0 - \theta_f = 10°$ is actually

$$\langle A_y \rangle = \frac{\int_{\theta_o}^{\theta_f} A_t(\theta)\rho(\theta)d\theta}{\int_{\theta_o}^{\theta_f} \rho(\theta)d\theta}, \tag{7}$$

where $\rho(\theta)$ is the probability distribution for a pion to scatter between θ and $\theta + d\theta$ and be detected by CHAOS. The angles θ_0, θ_f defined the lower and upper bounds of the bin.

The changing cross section is accounted for by calculating the statistically weighted scattering angle using the distribution of pion scattering angles observed during the measurement. Since the πp differential cross section, as well as CHAOS's geometrical acceptance and efficiencies, vary across individual bins, the pion's average angle is not necessarily the central value of the bin, i.e., $(\theta_f - \theta_0)/2$, but can differ from that value by 0.5°–3.3°.

E. Systematic errors

The advantage of asymmetry measurements is the cancellation of many factors associated with absolute cross sections experiments. For these measurements, there exist only two significant contributions to the systematic error, namely, the 3.7% uncertainty in the target polarization ($P^{\uparrow\downarrow}$) and the variations observed in the pion yield due to small sensitivities to the kinematic cuts. Three cut gates must be defined for each scattering bin of each measurement: proton angle, proton energy, and pion energy. Due to the finite resolution of the spectrometer, the yield histograms tend to have long tails, especially on the low-energy side. To estimate the error, the cut gates were altered, and slightly fluctuating asymmetries were observed. All three cut gates for each bin were made 10% wider and 10% narrower. As expected, the wider gates systematically lowered the analyzing powers, and the narrow gates caused random fluctuations in the value of A_y. The systematic error for each bin is determined to be half the difference between A_y using the wide and narrow gates.

TABLE I. Measured analyzing powers at 139, 117, and 98 MeV. The statistical and systematic errors are shown, but the 3.7% overall polarization normalization error is not. Standard and short track refer to the two trigger modes in which the data were acquired.

$\theta^{\pi}_{\text{c.m.}}$	$A_y(\theta) \pm \delta A_y(\text{stat}) \pm \delta A_y(\text{sys})$	$\theta^{\pi}_{\text{c.m.}}$	$A_y(\theta) \pm \delta A_y(\text{stat}) \pm \delta A_y(\text{sys})$
	138.9±0.7 MeV, π^+ (standard)		138.9±0.7 MeV, π^- (standard)
72.52	0.472±0.017±0.002	73.96	0.032±0.027±0.003
83.66	0.422±0.009±0.002	84.22	0.011±0.026±0.003
94.33	0.362±0.007±0.001	94.83	−0.060±0.022±0.001
104.44	0.245±0.007±0.001	104.63	−0.132±0.018±0.005
114.02	0.156±0.007±0.001	114.48	−0.193±0.013±0.004
123.21	0.085±0.005±0.001	123.21	−0.210±0.010±0.004
131.96	0.059±0.005±0.001	131.52	−0.202±0.011±0.001
140.47	0.039±0.004±0.001	140.55	−0.182±0.010±0.001
148.72	0.019±0.004±0.001	148.56	−0.159±0.010±0.001
156.67	0.004±0.004±0.001	156.67	−0.123±0.009±0.001
164.54	0.013±0.004±0.001	164.46	−0.080±0.010±0.001
172.30	0.008±0.004±0.001	172.07	−0.049±0.011±0.001
179.92	0.000±0.001±0.001	179.46	−0.028±0.015±0.005
	116.8±0.7 MeV π^- (standard)		98.0±0.7 MeV π^- (standard)
75.68	0.034±0.071±0.008		
84.35	0.042±0.030±0.007	85.04	0.014±0.084±0.001
93.88	−0.001±0.020±0.001	93.65	0.092±0.030±0.007
103.80	−0.056±0.016±0.002	103.28	0.001±0.023±0.001
113.62	−0.111±0.012±0.002	112.94	−0.069±0.020±0.002
122.49	−0.189±0.010±0.001	121.77	−0.132±0.013±0.003
131.75	−0.219±0.009±0.001	129.96	−0.169±0.013±0.001
139.93	−0.201±0.009±0.001	139.36	−0.203±0.013±0.002
148.03	−0.167±0.010±0.002	147.55	−0.167±0.015±0.001
156.33	−0.108±0.010±0.001	156.11	−0.134±0.014±0.002
164.31	−0.084±0.009±0.001	164.03	−0.082±0.015±0.001
171.87	−0.025±0.010±0.001	171.76	−0.052±0.017±0.004
179.38	−0.018±0.013±0.001	179.37	−0.012±0.020±0.003

These systematic errors, along with the statistical errors, are listed in the data tables. It should be noted that the systematic errors due to the cuts are much smaller than the statistical error, typically by a factor of 5–10.

IV. RESULTS

The data are shown in Figs. 2 and 3 and tabulated in Tables I and II. Only the statistical errors are shown in the figures. The 3.7% overall normalization uncertainty due to the target polarization measurements is not shown either in the tables or plots.

A. Comparison to previous work

There exist several measurements that overlap with the data of this work. Hofman *et al.* [14] published three π^+ data sets at 139.5 MeV, a single π^- set at 116.8 MeV and two π^- sets at 86.8 MeV (not shown). These data agree very well with the present work. In particular, the agreement at 139-MeV π^+ confirms the normalization of these previously published data. The Sevior *et al.* [9] π^- data set at 98 MeV is in good agreement. The Alder [10] data agree as well, but have large statistical errors.

B. Comparison to phase shift predictions

The present results are compared to the last published phase shift analyses of VPI/GWU group (SM95 [22]), the more recent (SM02) results of the same group [23] and those of the Karlsruhe group (KH80 [2,3]). Due to the proximity of a Barralet crossing point at 57 MeV, the π^- analyzing power predictions change rapidly with incident energy and angle. To properly evaluate the agreement with the existing phase shift solutions that are calculated at one energy, these solutions have been averaged (convoluted) with the incident beam energy profile and differential cross section given by the respective PWA's.

The momentum bite of the $M11$ channel varied from 1% (at 139 MeV) to 4% (full width) at 57 MeV. Individual pions are tracked using the GEANT based simulation to the center of the target. The resulting nearly Gaussian energy distribu-

TABLE II. Measured analyzing powers at 87, 67, and 57 MeV. The statistical and systematic errors are shown, but the 3.7% overall polarization normalization error is not.

$\theta^{\pi}_{\text{c.m.}}$	$A_y(\theta)\pm\delta A_y(\text{stat})\pm\delta A_y(\text{sys})$	$\theta^{\pi}_{\text{c.m.}}$	$A_y(\theta)\pm\delta A_y(\text{stat})\pm\delta A_y(\text{sys})$
	87.2±0.8 MeV, π^- (standard)		87.2±0.8 MeV, π^- (short track)
94.13	0.218±0.168±0.133	93.52	0.243±0.128±0.027
103.34	0.085±0.075±0.006	103.25	0.044±0.059±0.004
112.72	−0.046±0.057±0.007	112.82	0.029±0.035±0.003
121.58	−0.052±0.055±0.003	121.40	−0.070±0.031±0.007
130.16	−0.110±0.039±0.004	130.16	−0.093±0.031±0.003
138.99	−0.138±0.040±0.002	139.07	−0.172±0.030±0.005
147.56	−0.093±0.045±0.005	147.48	−0.152±0.032±0.003
156.02	−0.131±0.045±0.003	155.94	−0.138±0.033±0.003
163.99	−0.018±0.045±0.019	163.91	−0.099±0.034±0.001
171.87	−0.066±0.052±0.005	171.78	−0.017±0.038±0.004
179.36	0.012±0.062±0.022	179.36	−0.030±0.046±0.005
	66.9±0.9 MeV, π^- (standard)		66.9±0.9 MeV, π^- (short track)
		101.82	0.118±0.031±0.008
112.52	0.097±0.081±0.013	111.76	0.136±0.021±0.002
121.06	0.125±0.052±0.002	120.60	0.094±0.021±0.004
129.34	0.148±0.051±0.002	129.43	0.110±0.023±0.004
138.61	0.076±0.048±0.004	138.26	0.030±0.026±0.004
147.03	0.093±0.049±0.004	146.86	0.068±0.031±0.010
155.26	0.027±0.048±0.004	155.35	−0.002±0.034±0.005
163.35	−0.056±0.058±0.003	163.43	−0.062±0.051±0.003
171.26	0.031±0.077±0.030	171.50	−0.123±0.064±0.001
179.52	−0.107±0.107±0.020	179.19	−0.068±0.065±0.011

tion is fit. The weighted analyzing powers are calculated using

$$\langle A_y(\theta)\rangle = \frac{\int_0^\infty A_y(E,\theta)w(E,\theta)dE}{\int_0^\infty w(E,\theta)dE}, \tag{8}$$

where $A_y(E,\theta)$ is the analyzing power predicted by the phase shift analysis. The weighting factor $w(E,\theta)$ is defined by

$$w(E,\theta) = \psi(E)\frac{d\sigma}{d\Omega}(E,\theta), \tag{9}$$

where $\psi(E)$ is the Gaussian beam energy profile extracted from the Monte Carlo studies and $d\sigma/d\Omega$ is from the appropriate PWA. Beam energy uncertainties are also quoted in Tables I, II, and III.

The effect of this convolution at 57-MeV (Table III) π^- is shown in the bottom right panel of Fig. 3. There is a noticeable reduction in the analyzing power compared to that predicted at the central beam energy. Any phase shift solution that is compared to these measurements must take this effect into account. The effect is significant only near 170° at 57 MeV, but also noticeable at 67 MeV.

As can be seen from Figs. 2 and 3, the beam averaged SM95 phase shift (solid line) predictions agree very well with the present measurements, although the statistical errors at 67- and 87-MeV π^- are too large to draw strong conclusions. The agreement with the Karlsruhe solution KH80 (dashed lines) is poorer, especially at 98, 117, and 139 π^-. A direct comparison between all the data presented here and these two PWA solutions yields a χ^2_ν of 1.15 for SM95 and 6.72 for KH80. The newer SM02 solution (dotted line), which uses different Coulomb corrections and includes new

TABLE III. Measured analyzing powers at 57 MeV.

$\theta^{\pi}_{\text{c.m.}}$	$A_y(\theta)\pm\delta A_y(\text{stat})\pm\delta A_y(\text{sys})$
	57.2±0.9 MeV, π^- (short track)
101.74	0.178±0.029±0.001
111.95	0.175±0.019±0.001
120.33	0.187±0.015±0.001
129.38	0.205±0.015±0.001
137.99	0.183±0.017±0.001
146.55	0.210±0.020±0.004
155.01	0.212±0.025±0.001
162.99	0.282±0.034±0.008
170.95	0.252±0.135±0.025
179.67	0.064±0.097±0.029

pionic atom data, matches less well at all energies except 57 MeV.

V. SUMMARY

This work presented πp elastic analyzing powers at a single π^+ and six π^- energies below the $\Delta(1232)$ resonance. This is the first time that $\pi^- p$ analyzing power measurements below 87 MeV have been available. Systematic errors due to beam counting have been minimized by using the 360° acceptance of the CHAOS spectrometer. A special trigger detecting low momentum recoil protons allowed all data to be collected in coincidence mode, suppressing quasielastic backgrounds.

The 139-MeV π^+ data are in agreement with the previous data published by Hofman *et al.* and by Sevior *et al.* At the incident beam energies of 116, 98, 87, and 57 MeV, the present results clearly favor the SM95 PWA of the VPI Solidus GWU group over that of the KH80 analysis and strengthens the case for a higher value of the Σ term.

ACKNOWLEDGMENTS

We wish to thank TRIUMF for the support given to the experiment, in particular the efforts of the TRIUMF polarized target group. We also gratefully acknowledge financial support from the Natural Sciences and Engineering Research Council of Canada, the Istituto Nazionale di Fisica Nucleare of Italy, the Australian Research Council, the U.S. Department of Energy, the German ministry of education and research (Grant No. BMBF 06TÜ987), and the California State University Sacremento Foundation.

[1] T.P. Cheng and R. Dashen, Phys. Rev. Lett. **26**, 594 (1971).
[2] G. Hohler, in *Pion Nucleon Scattering*, edited by H. Schopper, Landolt-Börnstein, New Series, Group X, Vol. I, 9b2 (Springer Verlag, Berlin, 1983).
[3] R. Koch and E. Pietarinen, Nucl. Phys. **A336**, 331 (1980).
[4] M.M. Pavan and R.A. Arndt, in *Proceedings of the Eighth International Symposium on Meson-Nucleon Physics and the Structure of the Nucleon, Zuoz, Switzerland*, edited by D. Drechsel, G. Hohler, W. Kluge, H. Leutwyler, B.M.K. Nefkens, and H.-M. Staudenmaier [πN Newslett. **15**, 88 (1999)].
[5] Ulf-G. Meißner and G.R. Smith in *Chiral Dynamics 2000: Theory and Experiment* (Springer Verlag, New York, 2001).
[6] W.R. Gibbs, Li Ai, and W.B. Kaufmann, Phys. Rev. Lett. **74**, 3740 (1995).
[7] E. Matsinos, Report No. ETHZ-IPP PR-97-02, 1997 (unpublished).
[8] G.R. Smith *et al.*, TRIUMF Report E778, 1996.
[9] M.E. Sevior *et al.*, Phys. Rev. C **40**, 2780 (1989).
[10] J. Alder *et al.*, Phys. Rev. D **27**, 1040 (1983).
[11] B. Raue *et al.*, Phys. Rev. C **53**, 1005 (1996).
[12] C. Amsler, L. Dubal, G.H. Eaton, R. Frosch, S. Mango, F. Pozar, and U. Rohrer, Lett. Nuovo Cimento Soc. Ital. Fis. **15**, 209 (1976).
[13] R. Wieser *et al.*, Phys. Rev. C **54**, 1930 (1996).
[14] G.J. Hofman *et al.*, Phys. Rev. C **58**, 3484 (1998).
[15] P.P. Delheij and I. Sekachev, Nucl. Instrum. Methods Phys. Res. A **356**, 56 (1995).
[16] G.R. Smith *et al.*, Nucl. Instrum. Methods Phys. Res. A **362**, 349 (1995).
[17] G.J. Hofman, J.T. Brack, P.A. Amaudruz, and G.R. Smith, Nucl. Instrum. Methods Phys. Res. A **325**, 384 (1993).
[18] K.J. Raywood, S.J. McFarland, P.A. Amaudruz, G.R. Smith, and M.E. Sevior, Nucl. Instrum. Methods Phys. Res. A **357**, 296 (1995).
[19] M. Pavan *et al.*, Phys. Rev. C **64**, 064611 (2001).
[20] F. Bonutti, S. Buttazzoni, P. Camerini, N. Grion, and R. Rui, Nucl. Instrum. Methods Phys. Res. A **350**, 2136 (1994).
[21] S. Ritt and P.A. Amaudruz, Proceedings of the IEEE Conference on Real-Time Computer Applications in Nuclear Particle and Plasma Physics, Sante Fe, New Mexico, 1999.
[22] R.A. Arndt, I. Strakovsky, R. Workman, and M. Pavan, Phys. Rev. C **52**, 2120 (1995).
[23] The SM02 analysis is available at http://gwdac.phys.gwu.edu/